Drug Design, Development and Therapy Dovepress

Open Access Full Text Article ORIGINAL RESEARCH

Using Network Pharmacology and in vivo Experiments to Uncover the Mechanisms of Radix Paeoniae Rubra and Radix Angelicae Sinensis Granules in Treating Diabetes Mellitus-Induced Erectile Dysfunction

Jie Wang[1,*], Yingxue Guo[2,*], Jie Huang[2], Junfeng Yan[1], Jianxiong Ma[3,4]

[1]Zhejiang Hospital, Hangzhou, Zhejiang, 310000, People's Republic of China; [2]Second Clinical Medical College, Zhejiang Chinese Medical University, Hangzhou, Zhejiang, 310053, People's Republic of China; [3]The First Affiliated Hospital of Zhejiang Chinese Medical University (Zhejiang Provincial Hospital of Chinese Medicine), Hangzhou, Zhejiang, 310006, People's Republic of China; [4]The First Clinical Medical College, Zhejiang Chinese Medical University, Hangzhou, Zhejiang, 310053, People's Republic of China

*These authors contributed equally to this work

Correspondence: Jianxiong Ma, Department of Nephrology, The First Affiliated Hospital of Zhejiang Chinese Medical University (Zhejiang Provincial Hospital of Chinese Medicine), Hangzhou, Zhejiang, 310006, People's Republic of China, Email daxiong1990@zcmu.edu.cn; Junfeng Yan, Department of Urology, Zhejiang Hospital, Hangzhou, Zhejiang, 310000, People's Republic of China, Email kub@zju.edu.cn

Purpose: Diabetes mellitus-induced erectile dysfunction (DMED) lacks targeted therapies. This study investigates the mechanisms and targets of Radix Paeoniae Rubra and Radix Angelicae Sinensis Granules (RAG) in treating DMED using network pharmacology and animal models.

Methods: We identified RAG's active ingredients and potential targets from the Traditional Chinese Medicine Systems Pharmacology Database and Analysis Platform. DMED targets were obtained from GeneCards, OMIM, and PharmGKB. Common targets were identified using R, and interaction networks were built. Cytoscape was used to construct a drug-ingredient-disease-target network, and OmicShare tools performed Gene Ontology and KEGG pathway analyses. Molecular Operating Environment software assessed compound-core gene interactions. Additionally, animal models were used for validation.

Results: Twenty compounds and 25 common targets linked to vasodilation, protein secretion, apoptosis, and hypoxia were selected. Key pathways included HIF-1, MAPK, cAMP, and Ras. Six core genes (INS, CAT, BDNF, CASP3, CRP, HMOX1) were targeted by RAG. Molecular docking showed stable interactions with oleic acid, catechin, and butylated hydroxytoluene. RAG increased NO, intracavernous pressure, and improved penile histology in rats, upregulating eNOS, iNOS, HMOX1, and downregulating HIF-1.

Conclusion: RAG may treat DMED via the HIF-1α/HMOX1 pathway, offering a potential novel therapy for DMED.

Keywords: *Radix Paeoniae Rubra*, *Radix Angelicae Sinensis*, diabetes mellitus, erectile dysfunction, network pharmacology, hub genes, HIF-1 pathway

Introduction

Erectile dysfunction (ED) refers to the inability of the penis to achieve and maintain a sufficient erection to obtain a satisfactory sex life for at least six months. This ailment is one of the most common sexual dysfunctions in andrology[1] and seriously affects patients' quality of life and family stability. Diabetes mellitus (DM)-induced ED (DMED) is a class of ED, commonly brought on by DM. The incidence of ED in patients with DM is 3.5 times higher than that in patients without DM.[2] Moreover, ED appears 10–15 years earlier and is more serious in those with DM.[3] The reported incidence of DMED worldwide ranges from 20% to 75%.[4,5] The pathogenesis of DMED is complex and

Received: 27 August 2024
Accepted: 10 December 2024
Published: 25 December 2024

has not yet been fully clarified; however, it is known to be related to vascular endothelial dysfunction, cavernous smooth muscle volume atrophy, neuropathy, and tissue fibrosis.[6] Among them, vascular endothelial dysfunction is believed to be the primary pathophysiological basis of DMED. Although phosphodiesterase type 5 (PDE5) inhibitors are effective first-line medications for treating ED in clinical practice, many patients with DMED do not obtain satisfactory curative effects, and PDE5 inhibitors have no obvious therapeutic effect on diabetes.[6] Therefore, discovering new therapeutic approaches and better understanding the corresponding molecular mechanisms will help alleviate DMED.

Studies have shown that the endothelial dysfunction of DMED is the main cause of reduced nitric oxide (NO) synthesis and insufficient bioavailability.[7] Under physiological conditions, NO can be synthesized by three subtypes of NO synthase (NOS), including inducible NOS (iNOS), neuronal NOS (nNOS), and endothelial NOS (eNOS). When the vascular endothelial function is abnormal, insufficient secretion and decreased activity of eNOS are the main causes of poor reactions to PDE5 inhibitors.[8]

The activation of hypoxia-inducible factor (HIF-1α) by hyperglycemia and advanced glycation end products is widely accepted.[9] HIF-1α is an important signal transmission molecule in the ischemic and hypoxic environment,[10] which maintains the balance of the intracellular oxygen supply and demand, as well as the normal operation of glucose metabolism by regulating the expression of a variety of downstream regulatory factors, especially those in vascular endothelial cells and vascular smooth muscle cells.[11] In a DM rat model, the continuous increase of HIF-1α and advanced glycation products reduced the production of NOS, decreased the bioavailability of NO, and promoted fibrosis of the penile cavernous tissue and apoptosis of smooth muscle cells, ultimately causing ED.[12,13] Therefore, increasing NOS content and NO bioavailability and reducing hypoxia-inducible factors could be an effective approach for the treatment of DMED.

Since ancient times, a variety of medicinal plants have been the preferred choice for treating diabetes. Take Cassia glauca, for instance, its application in the treatment of diabetes has garnered widespread attention and research. For example, within the traditional medical systems of India, Cassia glauca is employed as a natural hypoglycemic agent, helping to control diabetes by improving insulin sensitivity and reducing blood sugar levels.[14] Similarly, Radix Paeoniae Rubra (RPR) and Radix Angelicae Sinensis (RAS) are also natural medicinal plants with a long history of use in China for treating blood disorders, diabetes, and other conditions. According to traditional Chinese medicine theory, RPR can clear heat, cool the blood, promote blood circulation, and remove blood stasis.[15] Moreover, pharmacological studies have confirmed that RPR has anti-thrombosis, anti-platelet aggregation, hypoglycemic, lipid-lowering, and anti-arteriosclerosis effects.[15,16] Meanwhile, RAS can replenish the blood, regulate menstruation, and relieve pain. RAS also has the properties of expanding blood vessels, increasing blood flow, inhibiting platelet aggregation, promoting the production of hemoglobin and red blood cells, lowering blood lipids, and fighting atherosclerosis.[17,18] Therefore, traditional Chinese medicine physicians usually use RPR and RAS in combination to promote blood circulation, relieve blood clotting, activate the veins, and relieve blood stasis in different tissues. This combination is also used in the treatment of diabetes complications.[19,20] However, because this herbal combination contains multiple components, targets, and pathways, current research on RPR + RAS is limited by the inability to comprehensively evaluate the mechanism of action. Therefore, it is of great significance to evaluate this combination systematically and comprehensively as well as excavate better ways of treating DMED.

Network pharmacology research has the characteristics of integrity and systematization. It is based on biological theory to construct networks of drugs, diseases, and targets, thus revealing the interactions between drug functions and body systems.[21] As traditional Chinese medicine compounds are multi-component and have multi-targets and multi-mechanisms, it is easier to elucidate their action mechanisms via network pharmacology of traditional Chinese medicine compounds.[22] In this study, network pharmacology was used to investigate the active ingredients of RPR + RAS granules (RAG) and explore the possible targets and mechanisms against DMED. Leveraging the advantages of network pharmacology, we further treated DMED rats with RAG, with the goal of clarifying the mechanisms by which the drug improves the histopathological damage to the corpus cavernosum of the penis and the related proteins in the pathway induced by cellular hypoxia. The flowchart of this research is shown in Figure 1.

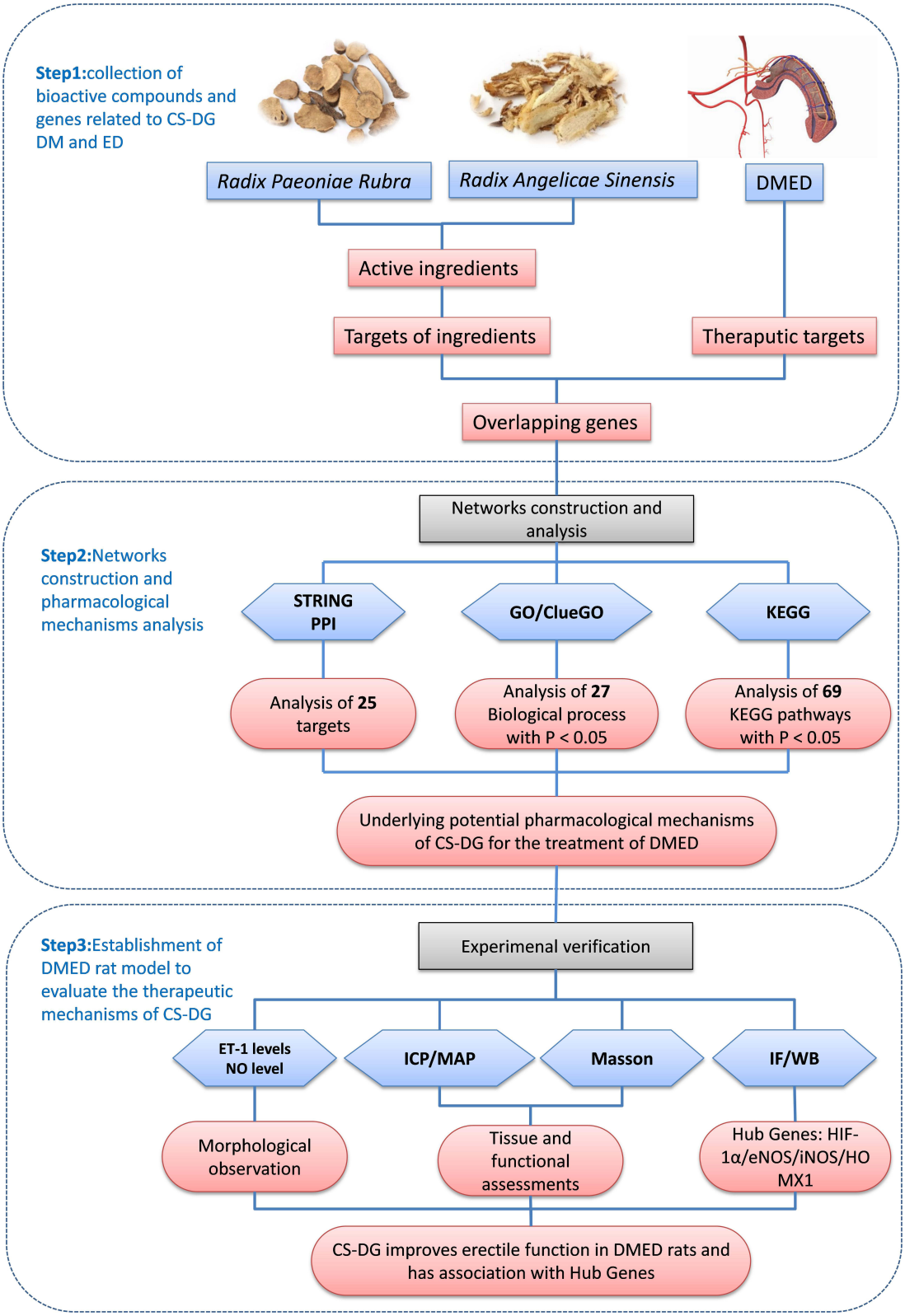

Figure 1 Flowchart showing the network pharmacology method used in this study and its experimental validation.

Materials and Methods

Identification of Active Components of RAG and Target Retrieval

The Traditional Chinese Medicine Systems Pharmacology (TCMSP) (http://lsp.nwu.edu.cn/tcmsp.php) database was used to retrieve the active ingredients of RPR and RAS. TCMSP is a commonly used Chinese medicine component database for the study of Chinese medicine network pharmacology,[23] which provides information bridging Chinese medicine with modern life sciences. The database contains information on more than 500 botanicals with more than 3000 compounds. We searched the database restricting the conditions of oral bioavailability to ≥ 30% and drug-likeness to ≥ 0.05 to obtain the biologically active components of RPR and RAS.

Prediction of RAG Targets

The targets of the active ingredients present in RAG were also retrieved from TCMSP database. The UniProt database (http://www.uniprot.org) was used to convert target protein names to gene names uniformly in order to process the data in a standardized manner.

Disease Targets of DMED

The relevant targets of DMED came from the following comprehensive disease-related data platforms: OMIM (https://www.omim.org/), GeneCards (https://www.genecards.org/), and PharmGkb (https://www.pharmgkb.org/). Literature and experimental data on a wide range of complex diseases are included in these databases. The search terms were set to "Diabetes Mellitus" and "Erectile Dysfunction" separately, and the search results of the three platforms were summarized, combined, and deduplicated to obtain the targets of DMED.

Screening of Common Targets for Drugs and Diseases and Construction of Interaction Networks

The R software (version 3.6.4) was used to identify common targets of drugs and diseases. The STRING platform (https://string-db.org/) was used to construct protein-protein interaction (PPI) networks of common targets, with "medium confidence" (> 0.4) as the minimum interaction threshold. Moreover, the R software was utilized to count the frequency of occurrence and to create a histogram. The Bioconductor websites were used to download all R packages. Additionally, the network of drug-ingredient-disease-target interaction was constructed using Cytoscape software 3.7.1 (https://cytoscape.org/), allowing us to visually represent the complex relationships between RAG, its active ingredients, and the targets implicated in DMED, with nodes of different colors and shapes representing diseases, drugs, active ingredients, and interaction targets to facilitate the interpretation of the network.

Biological Function and Pathway Enrichment Analyses

Using OmicShare platform tools (www.omicshare.com/tools), Gene Ontology analyses of core targets and Kyoto Encyclopedia of Genes and Genomes (KEGG) pathway enrichment analyses were performed. The results are presented in the form of bubble charts. A P-value < 0.05 indicated statistical significance. Based on the pathway enrichment factor, the impact of RAG on DMED was analyzed and possible mechanisms were explored. In addition, OmicShare was used to further analyze the results of GO and KEGG analyses; the results are presented as enrichment circle graphs and bar graphs.

Molecular Docking

The three-dimensional (3D) structure of the target protein can be downloaded from Protein Data Bank (PDB): BDNF (PDB ID: 1B8M, 2.75 Å), CASP3 (PDB ID: 3KJF, 2.00 Å), CAT (PDB ID: 1DGH, 2.00 Å), CRP (PDB ID: 3PVN, 1.98 Å), INS (PDB ID: 6SOF, 4.30 Å), and HMOX1 (PDB ID: 1S13, 2.29 Å). The structures of (+)-catechin, oleic acid, butylated hydroxytoluene acid, and beta-sitosterol compounds isolated from RPR or RAS were obtained from the PubChem database (https://pubchem.ncbi.nlm.nih.gov), which were used to further estimated the molecular binding capacity between these compounds and target proteins. Subsequently, the downloaded chemical structures were converted into 3D structures and their energies were minimized using the Molecular Operating Environment (MOE) 2015.10

software. Molecular docking was performed using MOE to analyze and compare the combined effects of BDNF, CASP3, CAT, CRP, INS, and HMOX1 compounds and crystal structures. Processing of target proteins was performed in MOE using standard procedures with default parameters. All protein structures were dehydrated, hydrogen atoms were added, and active binding sites were identified using the Sit Finder or by specifying atoms of natural ligands prior to calculations. The free energy of ligand binding (ΔGb) was evaluated in the MOE software, and the pose was saved. The optimal pose (ΔGb) with the lowest binding energy to the hydrogen atom was selected as the output result. We aim to estimate the molecular binding capacity between these compounds and proteins. This information is crucial for understanding the potential therapeutic effects of RAG on DMED.

Single-Cell Sequencing Analysis

To further substantiate the influence of HIF1A in erectile dysfunction (ED), we conducted an in-depth analysis of single-cell sequencing data. These data were sourced from the Gene Expression Omnibus (GEO) database under the accession number GSE206528.17 Our study encompassed a total of five samples: three from the unaffected tissue margins of penile cancer resections, representing the control group. These individuals exhibited regular erectile function, including spontaneous erections and those occurring in the early morning hours. The remaining two samples were derived from patients diagnosed with diabetes mellitus erectile dysfunction (DMED), who had undergone biopsies during artificial cavernous implantation. These patients had a history of type 1 diabetes spanning a minimum of a decade and maintained well-regulated blood glucose levels preoperatively. For data processing, we employed the Seurat package for quality assurance, data clustering, and graphical representation. Additionally, CellMarker 2.0 was utilized to identify and label signature genes. A comparative analysis was performed to discern the variations in cell proportions, marker gene expression, and HIF1A levels between the two cohorts. According to Item 1 of Article 32 of the Measures for Ethical Review of Life Science and Medical Research Involving Human Subjects, dated February 18, 2023, China, the data we use is sourced from the GEO database, where all data has undergone ethical review and obtained informed consent from patients. Our research meets the conditions for exemption from ethical approval.

RAG Preparation

RAG consisted of RPR granules (15 g) and RAS granules (15 g). RPR granules were formula granules made from the dried roots of Ranunculaceae *Paeonia lactiflora* Pall.; RAS granules were formula granules made from the dried roots of Umbelliferae *Angelica sinensis* (Oliv). Diels. The batch numbers of RPP and RAS production were ZBT1-24-80 and ZBT1-24-134, respectively. All of these granules were provided and appraised by Zhejiang Huisong Pharmaceutical Co., Ltd. All drugs were prepared according to the 2015 edition of the Chinese Pharmacopoeia. RAG was sealed and stored in a cool and dry environment until further use. The appraisal was completed by Professor Chen Hongshu at the Zhejiang Hospital of Traditional Chinese Medicine.

Composition Analysis of RAG

To clearly identify the active components of RAG, the compositions of RPR and RAS were determined using ultra-high-performance liquid chromatography quadrupole time-of-flight mass spectrometry (UHPLC-QTOF-MS/MS). Pharmaceutical component analysis was performed on a Waters ACQUITY UHPLC System with binary solvent manager using ACQUITY BEH C18 Columns (100 × 2.1 mm, 1.7 μm, Waters Corporation, Milford, MA, USA). The mobile phase contained 0.1% formic acid in acetonitrile (A) and 0.1% formic acid in water (B) with the following gradient changes: 0~2 minutes, 99% B; 2~12 minutes, 55~99% B; and 12~17 min, 15~55% B; 1.0 μL injection volume, 0.3 mL/min flow rate, 30 °C column temperature. MS analysis was performed on a Waters G2 QTOF™ system (Waters MS Technologies, Manchester, UK).

Experimental Animals and Housing

Eight-week-old male Sprague Dawley (SD) rats (180~200 g) were purchased from the Laboratory Animal Center of Zhejiang Chinese Medicine University (Certificate No.: SYXK 2021, Hangzhou, Zhejiang Province, China city). All rats were specific pathogen-free (SPF) grade. The rats were kept in a laboratory environment at 24 ± 2 °C, 45~55% relative

humidity, and a natural alternation between day and night (12 h/12 h). Food and water were provided to all rats with free access. The study was conducted by the National Institutes of Health guidelines on the use of experimental animals. The animal study was approved by the Animal Care and Use Committee of the Zhejiang Chinese Medicine University (20220411–13).

Establishment of DMED Rat Model and RAG Treatment

All 40 rats used in the experiment were fed adaptively for one week. Thirty rats were randomly selected to induce diabetes by maintaining a high-fat diet for one month. After a 12 h fast, the rats were intraperitoneally injected with streptozotocin (60 mg/kg, Beyotime Institute of Biotechnology, Shanghai, China). The remaining 10 age-matched SD rats were injected with an equal volume of citrate buffer and used as controls. A blood glucose meter (ACCU-CHEK Performa; Roche Diagnostics) was used to measure blood glucose levels in the tail blood after 72 hours, and 25 rats with constant fasting blood glucose > 16.7 mmol/L were classified as diabetic rats. After eight weeks, the DMED rats were screened using the apomorphine (APO)-induced erection test to confirm ED. APO hydrochloride hydrate (Sigma-Aldrich) was subcutaneously injected at a dose of 100 μg/kg. Ultimately, 20 DMED rats without apparent erectile response within 30 minutes were selected and randomly assigned into a model group (n = 10) or a RAG-intervention group (n = 10). Rats in the RAG group were administered RAG at a dose of 5.4 g/kg/day (equivalent to 17.8 g/kg of crude drug), and the control and model groups received physiological saline for four consecutive weeks. The body weight and fasting blood glucose levels of all the experimental rats were measured once a week after a 12-hour fasting.

Endothelial Function Assessment

The purpose of measuring serum ET-1 levels was to assess endothelial dysfunction, a key factor in DMED. Serum ET-1 levels were detected according to the instructions of the kit (EU0205, Wuhan Fine Biotech Co., Ltd., Wuhan, China). Plasma was collected with anticoagulant, followed by centrifugation at 1000 rpm for 15 min at 2~8 °C. The supernatant was collected overnight for analysis. NO is a vital endothelium-derived relaxing factor, and its quantification provides insights into vascular health and the potential effects of RAG on endothelial function in DMED. A one-step method was used to determine the serum NO level according to the instructions of the NO determination kit (A013-2-1, Nanjing Jiancheng Bioengineering Research Institute Co., Ltd., China). Before measurement, we collected 100 μL of serum stock solution, added 200 μL of reagent, and mixed both.

Erectile Function Assessment

Erectile function assessment was performed on all SD rats after four weeks of treatments. Rats were anesthetized with sodium pentobarbital, and systemic blood pressure was measured via carotid artery cannulation. Subsequently, the rat abdomen was incised, the bilateral cavernous nerves were isolated, and electrical stimulation was performed with bipolar electrodes (5.0 Volt, 15 hz, 5 ms pulse interval, 60s duration time, and 5 min interval between each electrical stimulation). Intra-cavernous pressure (ICP) and mean arterial pressure (MAP) were continuously recorded using the MP160 pressure sensor acquisition system (Biopac Systems Inc., Goleta, CA, USA). The maximum ICP (max ICP), max ICP to MAP ratio (max ICP/MAP), and ICP rising rate (slope) were used as the evaluation criteria for erectile function in rats.

Morphological Observation

After the erectile function test was completed, the entire penile tissue was harvested from each rat under pentobarbital sodium anesthesia. The corpus cavernosum tissue was transected into two sections, and the penile segment used for pathological staining was fixed with 4% paraformaldehyde. The rest of the penile tissue was frozen in liquid nitrogen and stored at −80 °C for further analysis. The rats were euthanized after tissue collection. Masson's trichrome staining (Solarbio, Beijing, China) was used to determine the ratio of smooth muscle to collagen in rat cavernous tissue sections. Penile histopathological images were obtained using a NanoZoomer S60 digital camera (HAMAMATSU, Shizuoka prefecture, Japan). Smooth muscle cells are shown in red, and collagen fibers are shown in blue. Masson's trichrome-stained images of all tissues were analyzed using ImagePro Plus 6.0 software (Media Cybernetics, Rockville, MD, USA). Tunel staining (share-bio, Shanghai, China) is utilized to ascertain the apoptotic status of rat cavernous smooth muscle

cells. Images are captured using the NanoZoomer S60 digital camera, where the cell nuclei are displayed as blue fluorescence, and the red fluorescence indicates apoptotic cells. Morphological observations can determine the changes in the penile corpus cavernosum structure of DMED rats and assess the therapeutic efficacy of RAG.

Immunofluorescence (IF) and Western Blotting (WB)

The purpose of using IF on corpus cavernosum tissue sections was to visualize the protein expression and localization of key markers associated with DMED pathology. The corpus cavernosum tissue was sectioned and stained with IF. Sections were incubated with rabbit primary antibodies, including anti-HIF-1α (1:200), anti-eNOS (1:200), anti-iNOS (1:200), anti-HMOX1 (1:200), and anti-β-actin (1:200) overnight (18 h). Next, sections were immersed in Alexa Fluor 488-conjugated secondary antibody (1:500), and nuclei were stained with 4′,6-dimidyl-2-phenylindole. IF analysis was performed using ImagePro Plus 6.0 software (Media Cybernetics, Bethesda, MD, USA). Western blotting (WB) was employed to quantify the protein expression levels of the same markers in penile tissues. The penile tissues of each group (100 mg) were homogenized for at least 30 minutes on ice with RIPA lysis buffer. A bicinchoninic acid protein detection kit (BCA, Beyotime Co., Ltd. China) was used to determine the total protein concentration of each protein sample. The protein samples (50 μg per sample) were separated using SDS-PAGE at the appropriate concentration and electrotransferred to polyvinylidene fluoride (PVDF) membranes (Bio-Rad Laboratories, Hercules, CA, USA). After blocking with 5% skim milk for 2 h at 25–30 °C, the PVDF membranes were incubated with the following primary antibodies overnight (18 h) at 4 °C: anti-HIF-1 (1:1000, CST, MA, USA), anti-eNOS (1:1000, Affinity, USA), anti-iNOS (1:1000, Affinity), anti-HMOX1 (1:1000, Affinity), and anti-β-actin (1:1000, Affinity). β-actin was used as the loading control. The PVDF membranes were further incubated with the corresponding secondary antibodies for 1.5 h. The bands were detected using enhanced chemiluminescence (ProteinSimple, USA). Finally, ImageJ software (1.48v) was used for semi-quantitative analysis. All experiments were repeated three times independently, with β-actin as the reference gene.

Statistical Analysis

All data are presented as mean ± standard deviation (SD). Statistical analyses were performed using SPSS 26.0 software. For comparisons between different groups, a one-way analysis of variance with Tukey's post-hoc test was employed. The significance level was set at $P < 0.05$. All graphs were generated using GraphPad Prism 8.0.

Results

Screening of Active Components of RAG

We identified 119 components in RPR and 125 components in RAS. According to the screening conditions, we identified 71 effective blood-active ingredients of the two drugs with oral bioavailability ≥ 30% and drug-likeness ≥ 0.05 (Table 1 and Supplementary Table S1). The main ingredients included paeonin, paeoniflorgenone, camphoric acid, senkyunolide D, 2-valerylbenzoic acid, and sedanolide, among others.

Table 1 Radix Angelicae Sinensis-Angelica Sinensis Bio-Active Ingredients Screened in TCMSP

	MOL NO.	Bio-Active Ingredients	OB%	DL
RPR	MOL007015	8-debenzoylpaeonidanin_qt	129.3	0.15
RPR	MOL007029	Paeonin,b_qt	105.45	0.08
RPR	MOL001935	(3aR,6S,7aR)-6-hydroxy-6-methyl-3-methylene-3a,4,7,7a-tetrahydrobenzofuran-2,5-dione	97.79	0.08
RPR	MOL001918	Paeoniflorgenone	87.59	0.37
RPR	MOL000244	()-Borneol	81.8	0.05
RPR	MOL007027	paeonin,a_qt	73.79	0.09

(*Continued*)

Table 1 (Continued).

	MOL NO.	Bio-Active Ingredients	OB%	DL
RPR	MOL007031	Paeonin,c_qt	72.7	0.09
RPR	MOL001925	Paeoniflorin_qt	68.18	0.4
RPR	MOL007016	Paeoniflorigenone	65.33	0.37
RPR	MOL006996	1-o-beta-d-glucopyranosy lpaeonisuffrone_qt	65.08	0.35
RAS	MOL008286	()-Camphoric acid	99.13	0.07
RAS	MOL002144	Senkyunolide-D	79.13	0.1
RAS	MOL008265	2-valerylbenzoic acid	78.26	0.06
RAS	MOL008259	2,6-di(phenyl) thiopyran-4-thione	69.13	0.15
RAS	MOL008252	Senkyunolide	68.28	0.07
RAS	MOL002098	3-Butylidene-7-hydroxyphthalide	62.68	0.08
RAS	MOL008251	Sedanolide	62.46	0.07
RAS	MOL002033	cis-THUJOPSENE	56.43	0.12
RAS	MOL008256	(3S)-3-butyl-3H-isobenzofuran-1-one	55.05	0.07
RAS	MOL008285	FERULIC ACID (CIS)	54.97	0.06

Note: Sort by OB value only list the top 10 compounds per drug.
Abbreviations: RPR, Radix Paeoniae Rubra; RAS, Radix Angelicae Sinensis.

Targets of Effective Active Ingredients in RAG

Using the TCMSP database, we identified 458 target points of active ingredients in RAG. Among them, succinic acid, oleic acid, methylbutenol, α-terpineol, and quercetin acted on 33, 30, 30, 19, and 77 targets, respectively. These active ingredients have more targets. The gene names of the target points were collected from the Uniprot database, and the invalid and duplicate targets were removed. A total of 107 target points of the effective active ingredients of RAG were obtained (Supplementary Table S2).

DMED-Related Genes and Drug–Ingredient–Genetics Interaction Network

We retrieved 1000 and 953 disease targets related to DM and ED, respectively, from the OMIM, GeneCards, and PharmGkb disease databases (according to a score ≥ 10). Using the R software, target points of the active ingredients in RAG were mapped, yielding 25 intersecting points (Figure 2A and Supplementary Table S3), which were regarded as the key targets for the RAG treatment of DMED. We input the active components of RAG and common target genes associated with drugs and diseases into Cytoscape 3.7.1 to construct a drug–ingredient–genetics (D-I-G) interaction network. The network contained 20 nodes representing the active ingredients of RAG and 25 nodes representing the disease targets. The D-I-G network is displayed in Figure 2B. Among them, NOS, CAT, CASP3, HMOX1, SOD, and MPO had relatively high representativeness, indicating great significance to the occurrence and development of DMED.

PPI Network of Disease-Drug Targets

A common target PPI network consisting of 25 nodes and 112 edges was constructed using the STRING plugin (Figure 2C and Supplementary Table S4). We used the R software to calculate the frequency of each target point and draw a bar graph (Figure 2D). Proteins with higher frequencies of interaction included INS, CAT, BDNF, CASP3, CRP, and HMOX1. Specifically, HMOX1 was the central protein of the entire network.

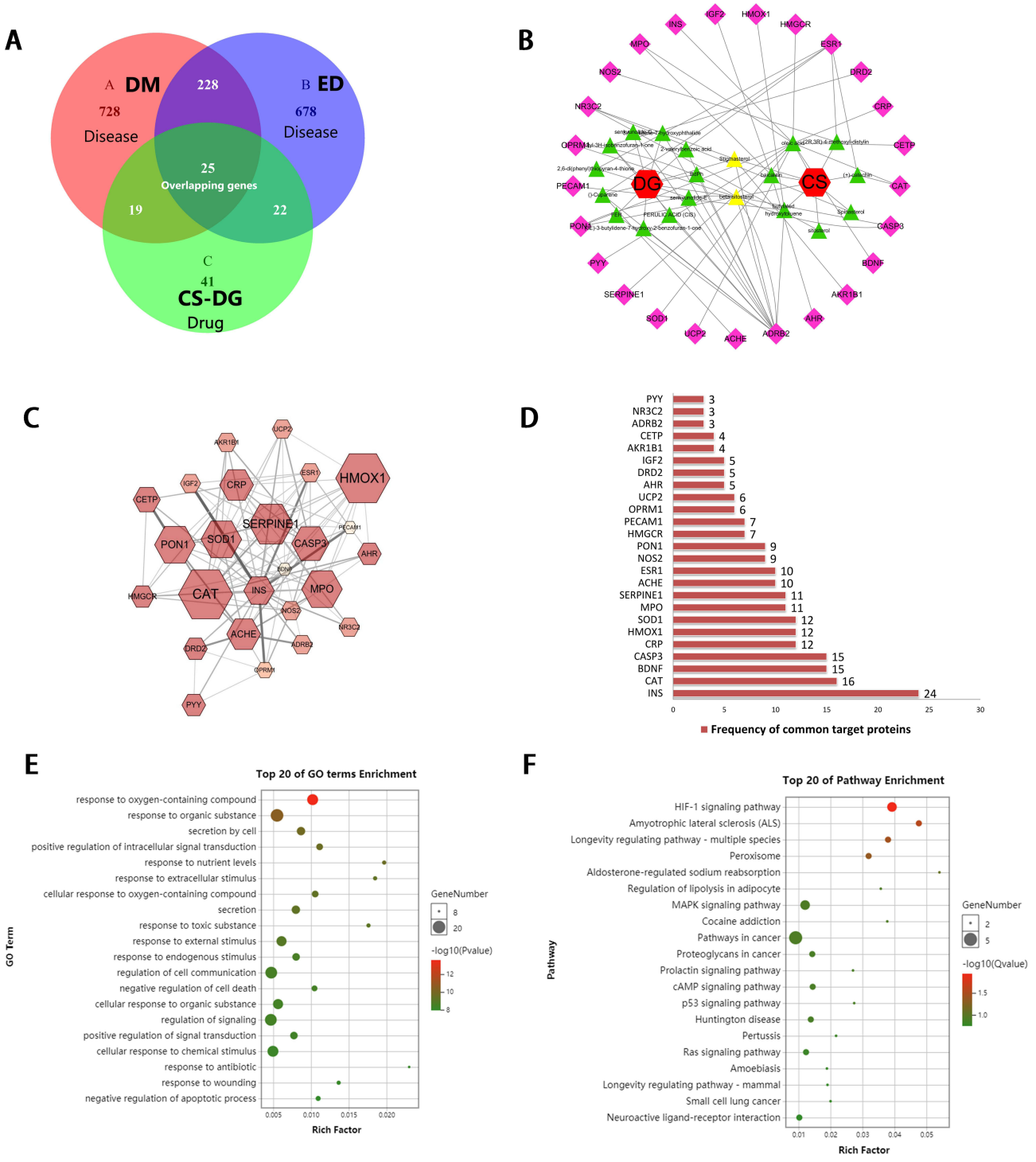

Figure 2 Drug-disease gene screening and bioinformatics analysis. (**A**) We found 25 genes shared between the drug and the disease. (**B**) A network diagram shows relationships: 25 purple nodes for shared genes, 20 green for RAG ingredients, 2 yellow for shared RPR and RAS ingredients, and an Orange node for RAG. Lines indicate possible interactions. (**C**) The PPI network for RAG's bioactive ingredients against DMED is shown, with thicker, darker lines for stronger interactions and larger, darker red nodes for more connected targets. (**D**) A bar graph displays the interaction frequency of the 25 most common target proteins in the PPI network, with the number of connections on the x-axis and the proteins on the y-axis. (**E**) The GO tool analysis shows the 25 DMED-related genes' enrichment in biological processes, with factors on the x-axis, categories on the y-axis, bubble size for gene count, and color intensity for significance. (**F**) KEGG pathway analysis indicates the genes' enrichment in signaling pathways, with factors on the x-axis, pathways on the y-axis, bubble size for gene count, and color intensity for significance.

https://doi.org/10.2147/DDDT.S493198 DovePress

Core Pathways of RAG in Treating DMED

GO analysis showed that DMED was mainly involved in biological processes such as vasodilation, protein secretion regulation, apoptosis, oxidation and anti-oxidation, and hypoxia induction (all $P < 0.01$; Figure 2E). Therefore, RAG can treat DMED by regulating a variety of complex biological processes.

In addition, KEGG pathway enrichment analysis of the above-mentioned core genes is shown in Figure 2F. Table 2 lists the top 20 signaling pathways after excluding extensive pathways. We identified 25 common targets that were mainly enriched in the HIF-1, MAPK, cAMP, and Ras signaling pathways, among others, suggesting that RAG may act on multiple pathways with complex interactions in the treatment of DMED. Redder nodes indicate smaller P-values, and larger nodes indicate a higher number of enrichment targets. Thus, large red nodes signify important signaling pathways.

Molecular Docking Results

The molecular docking scores of oleic acid combined with BDNF, CAT, CRP, and INS were −6.3901, −10.8577, −6.9114, and −107.9273 kcal/mol, respectively. The scores of beta-sitosterol-CASP3, (+)-catechin-CAT, and butylated hydroxytoluene acid-HMOX1 were −6.3707, −7.9781, and −5.565 0 kcal/mol, respectively (Table 3). Furthermore, multiple binding modes, including hydrogen bonds, H-π interactions, and π-π interactions, were observed in the docked compound. A variety of amino acid residues and core genes, including His 75, Arg 8112, Phe 207, Lys 8114, Tyr 8507, and Leu 8552, interacted with these compounds to synthesize proteins. The molecular docking patterns of the compound-hub genes are shown in Figure 3A–G. Table 3 shows the results of molecular docking between the active ingredient and the target gene.

Single-Cell Landscape in ED Patients

We employed an unsupervised graph-based clustering approach to classify the primary cell clusters and generated a comprehensive Uniform Manifold Approximation and Projection (UMAP) plot that illustrated the cellular composition (Figure 4A). Cells exhibiting similar gene expression profiles were annotated according to the expression of specific lineage markers. These included endothelial cells (clusters C0, C2), fibroblasts (C1, C5, C9), T cells (C8), macrophages (C7), smooth muscle cells (C3, C6, C10), and vascular smooth muscle cells (C4) (Figure 4B).The t-distributed stochastic neighbor embedding

Table 2 Result of Target Pathway Enrichment (Top 20)

Pathway ID	Pathway Name	Count	P value	Gene Name
ko04066	HIF-1 signaling pathway	4	9.94E-05	*NOS2/HOMX1/SERPINE1/INS*
ko05014	Amyotrophic lateral sclerosis (ALS)	3	0.000467	*CAT/SOD1/CASP3*
ko04213	Longevity regulating pathway - multiple species	3	0.000907	*CAT/SOD1/INS*
ko04146	Peroxisome	3	0.001501	*NOS2/CAT/SOD1*
ko04960	Aldosterone-regulated sodium reabsorption	2	0.003664	*NR3C2/INS*
ko05030	Cocaine addiction	2	0.007403	*DRD2/BDNF*
ko04010	MAPK signaling pathway	4	0.008029	*CASP3/IGF2/BDNF/INS*
ko04923	Regulation of lipolysis in adipocyte	2	0.008236	*ADRB2/INS*
ko05200	Pathways in cancer	5	0.009459	*NOS2/ESR1/HOMX1/CASP3/IGF2*
ko04115	p53 signaling pathway	2	0.013706	*SERPINE1/CASP3*
ko04024	cAMP signaling pathway	3	0.013817	*DRD2/ADRB2/BDNF*
ko04917	Prolactin signaling pathway	2	0.014066	*ESR1/INS*
ko05205	Proteoglycans in cancer	3	0.014177	*ESR1/CASP3/IGF2*
ko05016	Huntington disease	3	0.015477	*SOD1/CASP3/BDNF*
ko04014	Ras signaling pathway	3	0.02089	*IGF2/BDNF/INS*
ko05133	Pertussis	2	0.021227	*NOS2/CASP3*
ko05222	Small cell lung cancer	2	0.024807	*NOS2/CASP3*
ko04211	Longevity regulating pathway - mammal	2	0.027162	*CAT/INS*
ko05146	Amoebiasis	2	0.027643	*NOS2/CASP3*
ko04933	AGE-RAGE signaling pathway in diabetic complications	2	0.03162	*SERPINE1/CASP3*

Table 3 Interaction of Hub Genes with Compounds from Radix Paeoniae Rubra and Radix Angelicae Sinensis

Gene name	PDB ID	Herbs	Compound			H-Bonds		π-Interactions	
			Name	PubChem CID Compound	ΔGb	Type Amino Acid	Type Amino Acid	Amino Acid	Amino Acid
BDNF	1B8M	RPR	Oleic acid	445639	−6.3901	-	-	-	-
CAPS3	3KJF	RPR and RAS	Beta-sitosterol	12303645	−6.3707	-	-	-	-
CAT	1DGH	RPR and RAS	(+)-catechin	9064	−7.9781	-	-	pi-pi	His 75
CAT	1DGH	RPR	Oleic acid	445639	−10.8577	H-donor H-acceptor	Arg B-112 Arg B-112	-	-
CRP	3VPN	RPR	Oleic acid	445639	−6.9114	H- acceptor	Lys *B*-114	-	-
HMOX1	1S13	RPR	butylated hydroxytoluene	31404	-5.5655			H-pi	Phe 207
INS	6SOF	RPR	Oleic acid	445639	-107.9273	H-donor H-donor H-acceptor H-acceptor	Leu *E*-552 Leu *B*-552 Try *B*-507 Try *E*-507	-	-

Abbreviations: RPR, Radix Paeoniae Rubra; RAS, Radix Angelicae Sinensis.

(tSNE) map of the cells highlighted the expression patterns of several marker genes, such as VWF for endothelial cells, DCN for fibroblasts, ACTA2 for smooth muscle cells, TAGLN for vascular smooth muscle cells, CD86 for macrophages, and CD3D as a T cell marker. We utilized CellMarker 2.0 to identify these cellular markers, which facilitated the annotation and detailed commentary on the specific cell types present within our dataset (Figure 4C). Furthermore, the expression levels of HIF1A were evaluated in both diabetic and normal cells, demonstrating a significant difference between the two groups (Figure 4D). Additionally, HIF1A expression levels were found to vary across the different cell types, as depicted in Figure 4E and F.

Chemical Composition of RAG

UHPLC-QTOF-MS/MS was used to analyze the chemical characteristics of RAG. The SCIEX OS software was used to analyze the quality of the data. A total of 12 compounds were identified in the positive ion mode, and 28 compounds were identified in the negative ion mode using the first-order accurate mass of the compound, isotope distribution ratio, MS/MS data, and the TCM MS/MS library in the SCIEX OS software. Moreover, some compounds were identified in both modes. The compounds mainly consisted of glycosides, esters, and acids. Additionally, several compounds identified by UHPLC-QTOF-MS/MS were also identified from RPR and RAS screening in the TCMSP database (Supplementary Figure 1, Supplementary Table S5 and S6).

Effect of RAG on Physiological Markers and Endothelial Function in DMED Rats

Similar body weight was observed between the RAG-treated and non-treated DMED rats on days 7, 14, 21, and 28 ($P > 0.05$). However, the fasting blood glucose levels of rats in the treatment group on days 14, 21, and 28 were significantly lower than those in the model group ($P < 0.01$). Nonetheless, the overall blood glucose level was still significantly higher than that of the control group (Figure 5A and B). In addition, the serum NO level in the model group was significantly lower than that in the control group, and the ET-1 level was significantly increased ($P < 0.01$; Figure 5C and D). After the RAG intervention, the serum NO levels in the treatment group were significantly increased, while ET-1 levels were significantly reduced ($P < 0.01$).

Effect of RAG on Erectile Function in DMED Rats

We measured ICP and MAP in DMED rats at 0 and 5 V, respectively, to evaluate the effect of RAG on erectile function (Figure 6A). Figure 6B–D shows the max ICP, max ICP/MAP ratio, and the ICP rising rate (slope) of each group.

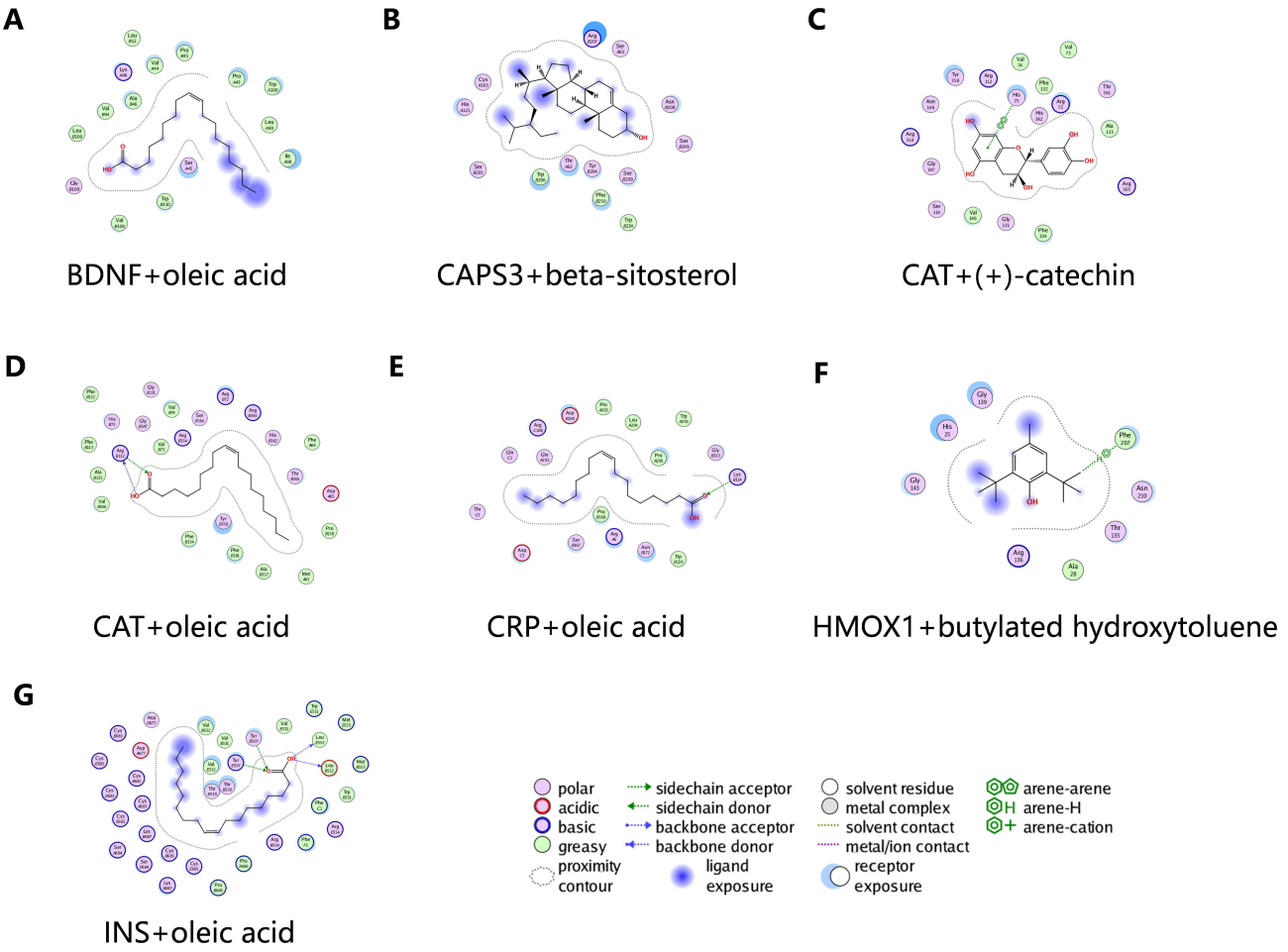

Figure 3 An analysis of the molecular docking of active ingredients in RAG with its target molecules. We selected four bioactive components from RAG and six common target proteins for molecular docking. The virtual molecular docking of oleic acid with BDNF, CAT, CRP, and INS is represented in (**A**), (**D**), (**E**), and (**F**), respectively. Virtual molecular docking of beta-sitosterol with CASP3 is represented in (**B**). Virtual molecular docking of (+)-catechin with CAT is represented by (**C**). The virtual molecular docking of butylated hydroxytoluene acid with HMOX1 is represented in (**G**).

Compared with that of the control rats, the max ICP/MAP ratio of DMED rats was significantly reduced ($P < 0.01$), indicating that the rat model of diabetes was successfully established. This ratio was significantly improved after RAG treatment, indicating that RAG treatment may improve the erectile function of DMED rats.

Pathological Changes in Penile Tissue

The penile tissue of the DMED group exhibited endothelial cells with pronounced swelling and plasma membrane damage, contrasting sharply with the intact state observed in the control group. Furthermore, the cavernous tissue's endothelial and smooth muscle cells in the DMED group displayed an irregular distribution, with their structural organization significantly disrupted. Notably, an excessive accumulation of collagen was evident within the cavernous tissue of the DMED rats, pointing towards profound tissue fibrosis in the penile region. Additionally, a starkly diminished smooth muscle to collagen ratio was detected in the muscle tissue of the DMED group when juxtaposed with the control group, with a statistically significant difference ($P < 0.001$). In contrast, the RAG intervention group demonstrated a marked increase in the quantity of endothelial cells and smooth muscle content, along with an elevated smooth muscle to collagen ratio ($P < 0.05$) when compared to the model group. These observations suggest that RAG treatment may ameliorate the pathological changes in penile tissue caused by DMED, as illustrated in Figure 7A. As shown in Figure 7B, through the Tunel staining technique, we observed a significant increase in the number of apoptotic cells in the penile cavernous tissue of the model group, and RAG intervention could effectively suppress the phenomenon of apoptosis in penile cavernous tissue under diabetic conditions.

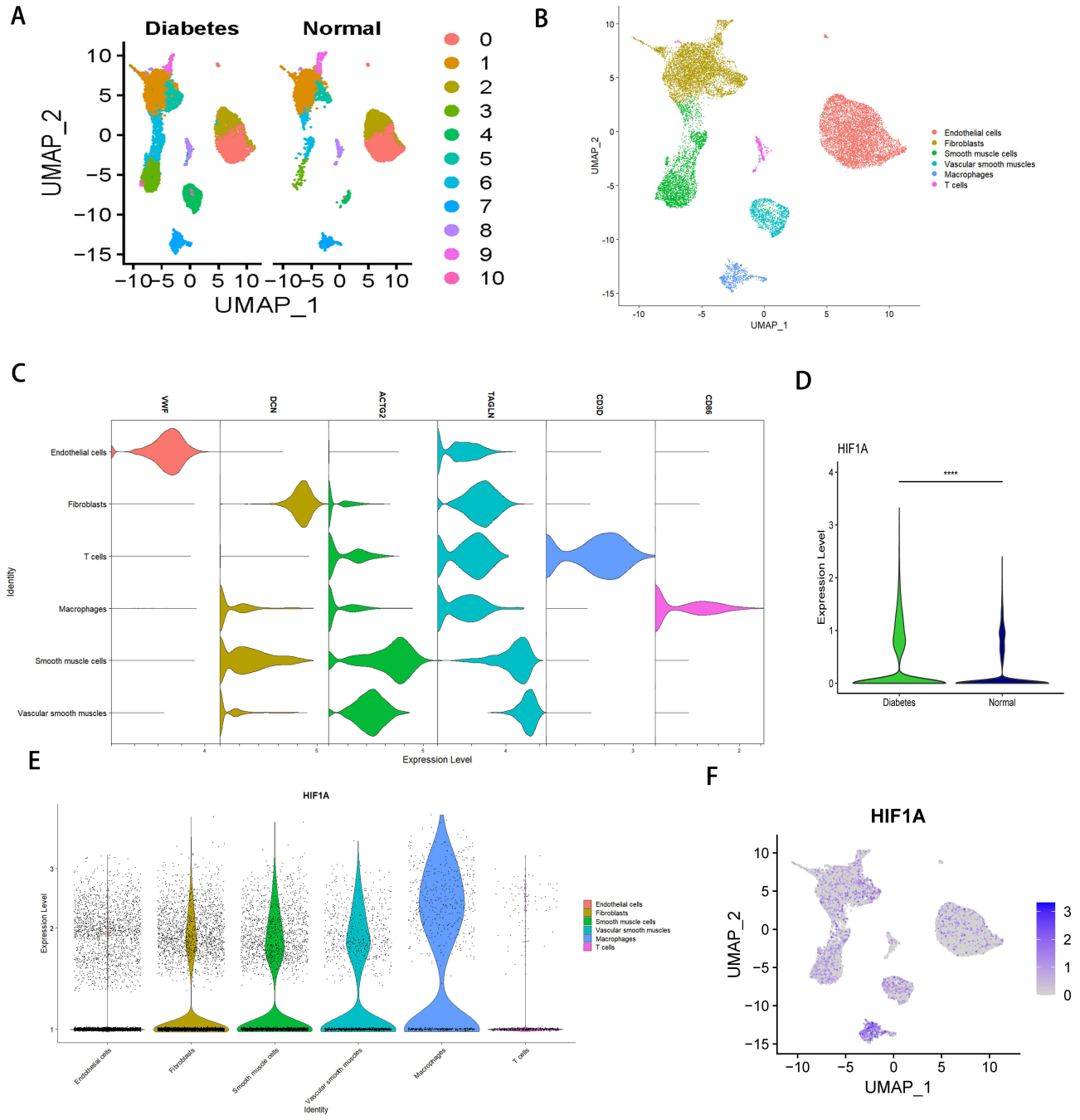

Figure 4 Single-cell sequencing revealed the global expression profile of diabetes mellitus-induced erectile dysfunction (DMED) patients. (**A**) The tSNE plots visually represent the cellular heterogeneity among the cavernosal cells from the five donors, offering a two-dimensional projection that captures the complex cellular relationships. (**B**) Post cell annotation, the tSNE plots are color-coded to distinguish between different cell types, providing a clear visual distinction of the cellular composition within the samples. (**C**) Utilize CellMarker 2.0 to identify cellular markers. (**D**) This comparative expression analysis of HIF1A is presented to highlight any significant disparities between the two groups, which could be indicative of the role of HIF1A in the development of erectile dysfunction in type 1 diabetes patients. (**E**) The expression patterns of HIF1A across the entire dataset of cavernosal cells are depicted, illustrating how HIF1A expression varies within the cellular populations. (**F**) The tSNE profiles of all cavernosal cells (CC cells) are annotated with HIF1A expression levels, offering a comprehensive view of the distribution and potential clustering of cells based on their HIF1A expression profiles.

Expression Levels of Core Genes in DMED Rats

To further explore the changes in the hub genes from DMED and the mechanism of action of RAG, we combined the PPI network interaction targets with the molecular docking results of the common drug-disease targets and selected hypoxic stress-related genes as validation targets. The protein expression levels of HIF-1α, eNOS, iNOS, and HMOX1

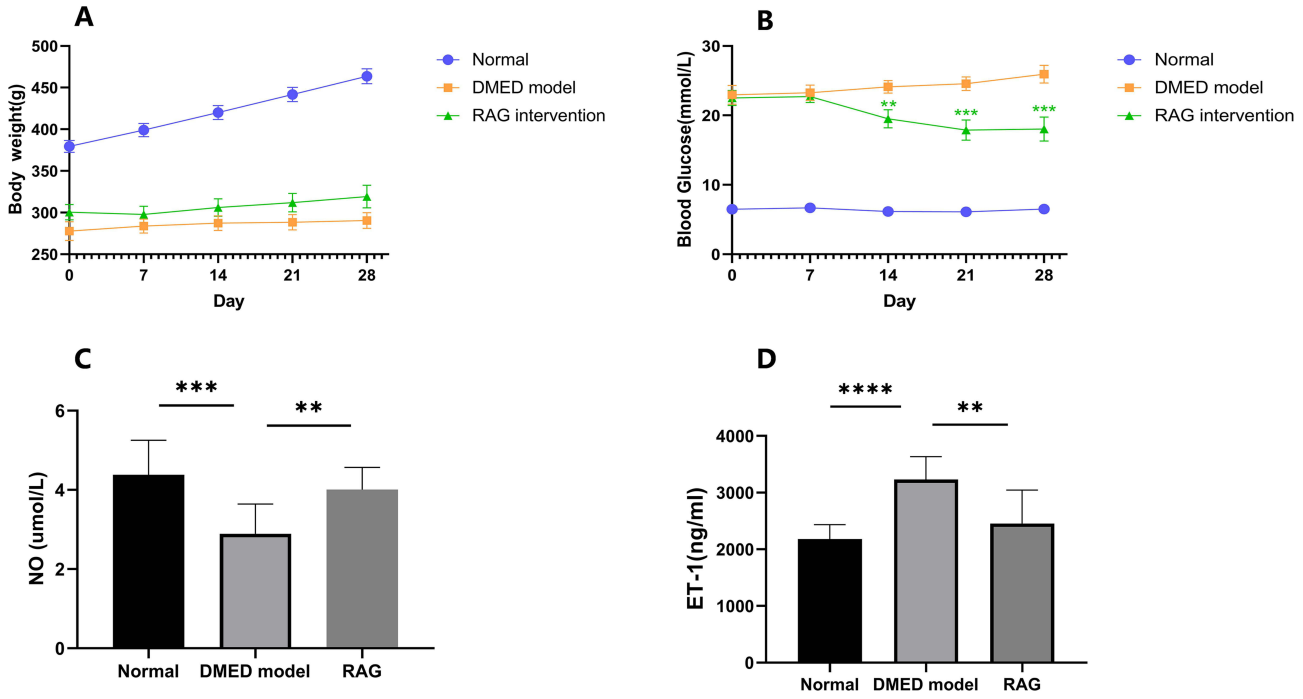

Figure 5 The effect of RAG on physiological markers and endothelial function in DMED rats. (**A**) and (**B**) Changes in body weight and fasting blood glucose of rats in each group after the start of treatment, respectively. The detection frequency was once a week. The blue point represents the control group, the Orange point represents the model group, and the green point represents the intervention group. The serum NO and ET-1 levels in the rats were represented in (**C**) and (**D**). $^{**}p < 0.01$, $^{***}p < 0.001$, $^{****}p < 0.0001$.

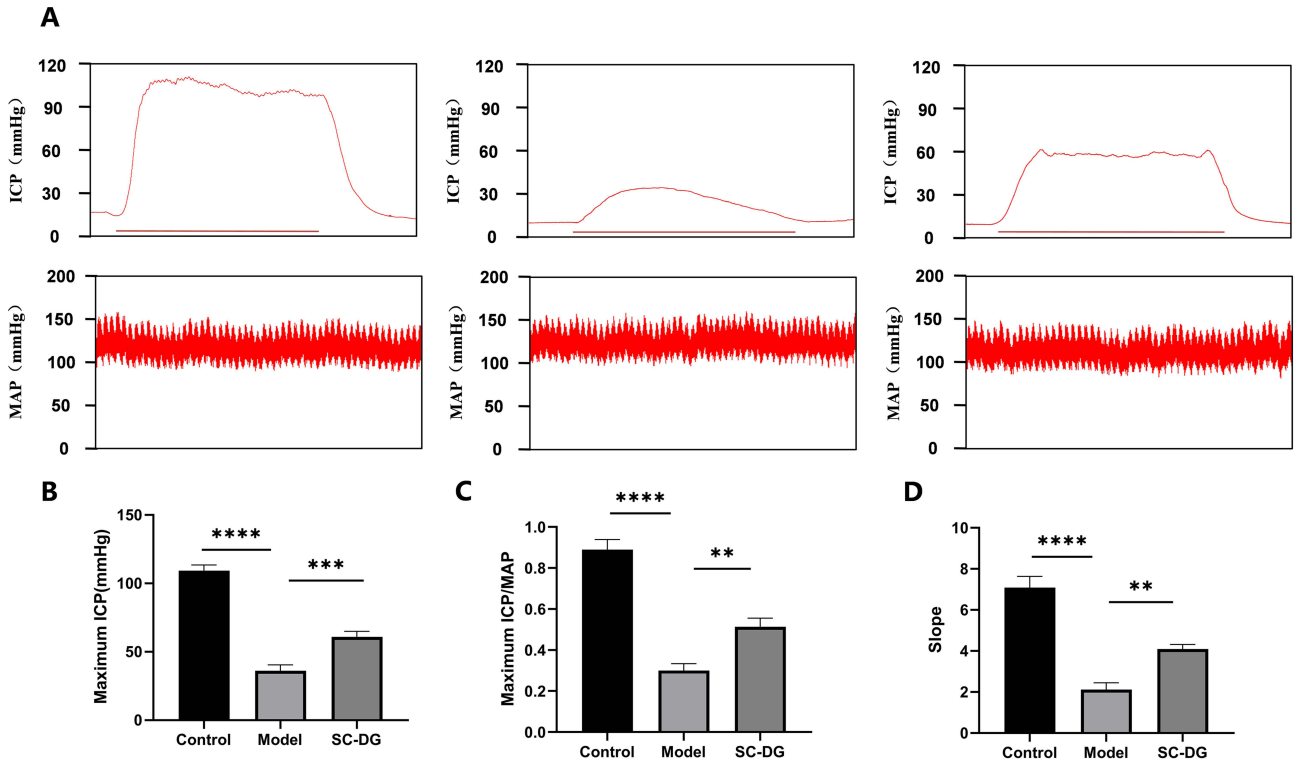

Figure 6 ICP and MAP detection results of rats in each group. (**A**) The detection results of ICP and MAP of the rats in each group; the ordinate is ICP and MAP (mmHg), the abscissa is time, and the horizontal line represents the duration of electrical stimulation. (**B**–**D**) Statistical results of maximal ICP, maximal ICP/MAP, and mean slope of post-stimulation ICP rise in each group (n = 5). $^{**}p < 0.01$, $^{***}p < 0.001$, $^{****}p < 0.0001$.

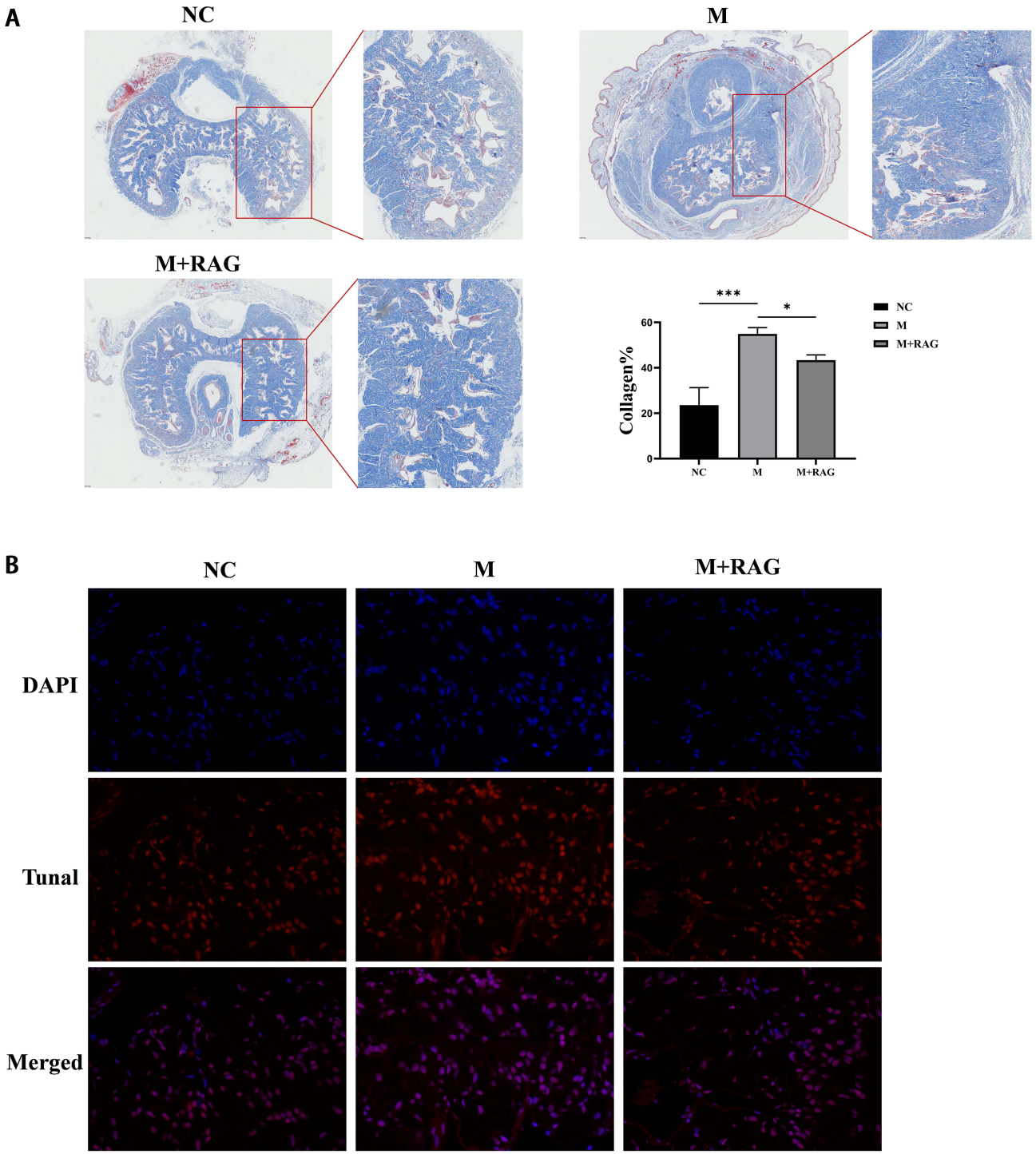

Figure 7 Masson's trichrome staining of penile mid-shaft specimens. (**A**) Representative Masson's trichrome staining of the corpus cavernosum (magnification ×100). Smooth muscles were stained in red, and collagen fibers were stained in blue. (**B**) The TUNEL assay demonstrated that RAG effectively mitigated the apoptosis of corporal smooth muscle cells (CCSMCs). The cells exhibited red fluorescence from the TUNEL reagent, indicating DNA damage, while the nuclei were counterstained with DAPI, presenting a blue fluorescence. *$p < 0.05$, ***$p < 0.001$.

were detected by IF and WB in penile tissues of DMED rats treated with RAG (Figure 8A and B). Compared with the control group, the expression level of HIF-1α in the DMED group was significantly increased ($P < 0.05$), and the expression levels of eNOS, iNOS, and HMOX1 were significantly decreased ($P < 0.01$, < 0.01, and < 0.05,

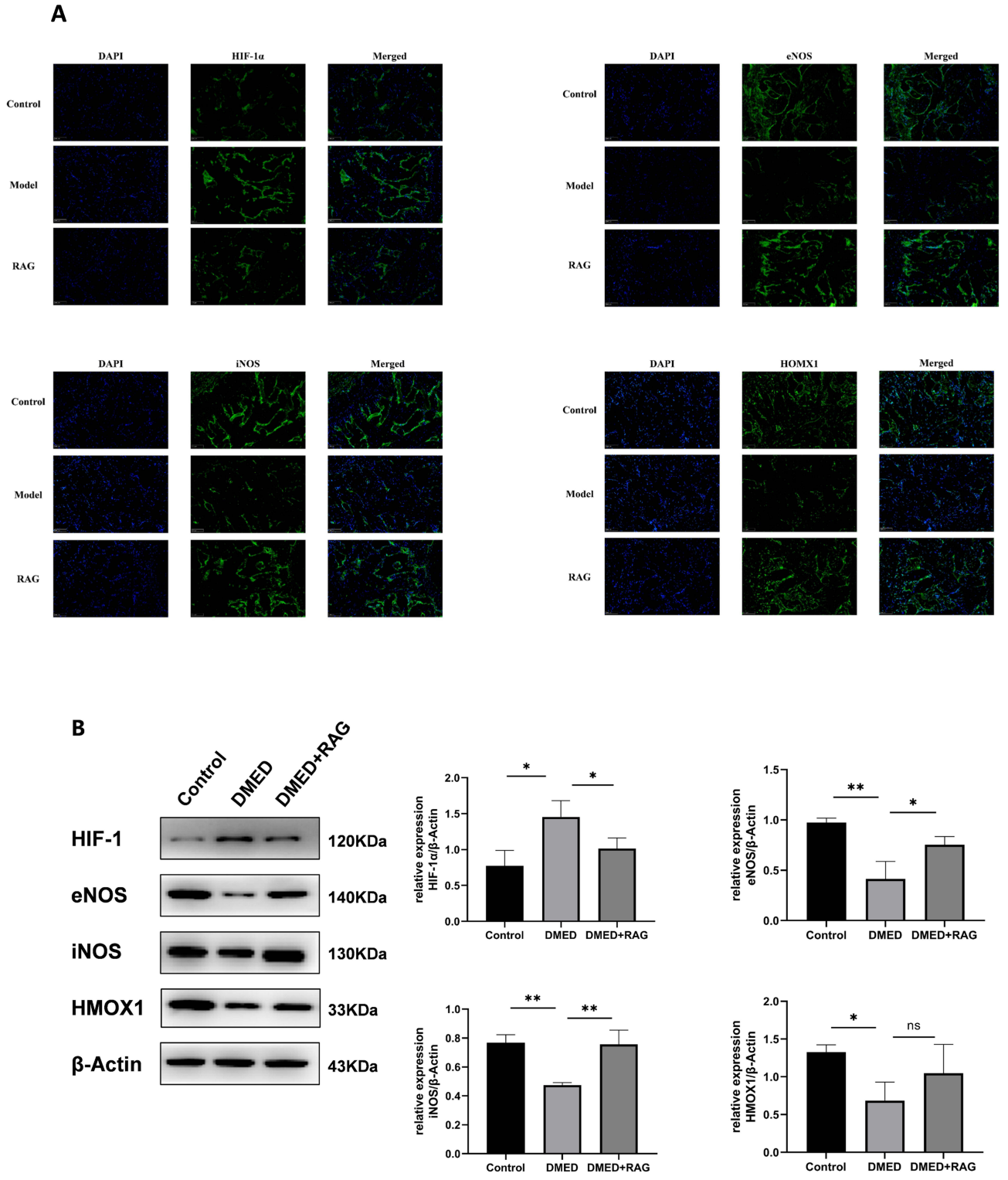

Figure 8 RAG treatment regulates the expression of hub genes in DMED rat corpus cavernosum. (**A**) Representative images of immunofluorescent staining of cavernosal tissue with anti-HIF-1α, anti-eNOS, anti-iNOS, and anti-HMOX1 in various groups. (**B**) HIF-1α, eNOS, iNOS, and HMOX1 protein expression in cavernous tissues from the three groups were determined by Western blotting. Error bars: mean SD; n = 5–6 in each group. NS: not significant ($p \geq 0.05$), *$p < 0.05$, **$p < 0.01$.

respectively). After RAG intervention, the expression of eNOS and iNOS in the treatment group were significantly increased ($P < 0.05$ and < 0.01, respectively), while that of HIF-1 was significantly decreased ($P < 0.05$). Representative IF images confirmed this trend.

Discussion

Due to its complexity, the pathogenesis of DMED has not been fully elucidated, hindering clinical treatment. Moreover, more effective targets of combination therapy, in addition to those of PDE5 inhibitors, must be identified. Studies have confirmed that DMED is caused by various factors such as oxidative stress, advanced glycation end products, and receptors for advanced glycation end products, endothelial dysfunction, peripheral neuropathy, and penile fibrosis.[24] Furthermore, according to traditional Chinese medicine, the pathological basis of DM consists of a "deficiency of both qi and yin;" thus, toxin blockage and blood stasis are thought to be the key to diabetic vascular complications. As a result, traditional Chinese medicine employs RPR and RAS as the representative drugs for promoting blood circulation and removing blood stasis. The combined use of the two drugs can strengthen their effects and produce better curative effects for diseases with collateral stasis. Furthermore, many pharmacological studies have confirmed that the combined use of RPR and RAS can improve neurodegenerative diseases, inhibit renal tubular epithelial–mesenchymal transition induced by high glucose, reduce renal damage mediated by advanced glycation end products, and regulate oxidative stress.[19,25,26]

Due to the complexity of traditional Chinese medicine, multiple components are often involved in the efficacy of such medicines, complicating research regarding such compounds. Therefore, we used network pharmacology for comprehensive analysis, screened out reliable targets, and performed experimental verification to elucidate the mechanism of RAG treatment for DMED.

This study demonstrated that the effective active ingredients of RAG mainly included paeoniflorin, albiflorin, paeoniflorigenone, senkyunolide, beta-sitosterol, oleic acid, and sedanolide. Among them, beta-sitosterol, oleic acid, butylated hydroxytoluene, and (+)-catechin were the core nodes in the drug-ingredient-disease-target network, exhibiting higher binding power with common core targets in further molecular docking assessments. Thus, these effective active ingredients may play an important role in the treatment of DMED. Studies have shown that the various components of RAG improve vascular endothelial function, reduce the specific viscosity of the blood, reduce vascular resistance, expand capillaries, relieve arteriole spasm, improve microcirculation, reduce vascular inflammation, and reduce the occurrence of cardiovascular events.[27–29] Vascular endothelial injury and dysfunction are also important links in the occurrence and development of DMED. Our results show that RAG promotes NO release in the serum and reduces the level of ET-1, which can improve the function of the vascular endothelium. In addition, many ingredients of RAG regulate blood sugar, allowing the drug to improve the function of blood vessels while treating some underlying diseases.[30,31] In addition, we confirmed that the fasting blood glucose levels of DMED rats reduced after 14 days of RAG treatment but did not reach the normal level.

On the basis of the 25 disease-drug targets, PPI network and KEGG pathway enrichment analyses were performed to identify RAG targets for DMED treatment. These modular target genes mainly had regulatory effects on HIF-1, MAPK, cAMP, Ras, and other signaling pathways related to the pathogenesis of DMED. In addition, six targets were hub genes according to their degree values, including BDNF, CASP3, CAT, CRP, INS, and HMOX1, which could be related to beta-sitosterol, oleic acid, butylated hydroxytoluene, and (+)-catechin. Our docking simulation showed that oleic acid, beta-sitosterol, and (+)-catechin had a relatively stable binding affinity to the hub genes.

Evidence suggests that HIF-1 overexpression plays an important role in the development of DM and ED. Moreover, the HIF-1 signaling pathway plays a key role in the development of fibrosis and smooth muscle cell apoptosis induced by hypoxia.[32,33] When glucose uptake or glycolysis is partially inhibited, hypoxia-induced apoptosis is gradually initiated, leading to corresponding tissue and organ dysfunction.[34] Similarly, hypoxia-induced expression of hypoxia-inducible factor-1 reduces endothelial nitric oxide synthase (eNOS) expression in isolated rat cavernosal tissue. RAG has the ability to alleviate tissue hypoxia and suppress the expression of HIF-1. Enhancing the secretion of eNOS, generates NO, which plays a pivotal role in regulating vasodilation and sustaining normal erectile function.

Results from the combined network pharmacology and bioinformatics analysis showed that HMOX1 was the central protein of the entire network, indicating that it may have higher binding activity with the active ingredients of RAG and act as a potential target of RAG in the treatment of DMED. Previous studies have confirmed that HMOX1 is a stress-induced enzyme that breaks down heme into biliverdin, carbon monoxide, and iron in the body. Since excess free heme sensitizes cells and leads to apoptosis, the expression of HMOX1 can reduce programmed cell death, showing

a protective effect on cells.[35] As an important downstream target of HIF-1, HMOX1 can be induced by activated HIF-1 in large quantities to cope with various adverse conditions, such as ischemia, hypoxia, inflammation, abnormal glucose metabolism, and other damage to tissues and organs.[36] A study showed that HMOX1 knockout mice had impaired HIF-1α stability and glucose utilization. Additionally, HMOX1 acts both downstream and upstream of HIF-1α and protects local tissue from ischemia-mediated damage.[37] Similarly, another study showed that activation of HIF-1 markedly induces HMOX-1 expression after cardiac surgery, resulting in reduced production of pro-inflammatory chemokines in the microvascular endothelium.[38] In line with these findings, the latest research indicates that upregulating HMOX1 may repair high glucose-induced endothelial cell damage in the corpus cavernosum by modulating ferroptosis and oxidative stress, thereby restoring erectile function in DMED rats.[39]

The findings from our DMED model study showed that RAG could relieve ED in rats, ameliorate erectile tissue reactivity and ICP, improve the arrangement of endothelial cells and smooth muscle cells, and reverse penile histopathological damage and the smooth muscle/collagen ratio. RAG also significantly reduced the expression of HIF-1 and the levels of hypoxic stress in the penile cavernous tissue and increased the secretion of eNOS and nNOS as well as the expression of HMOX1. These results suggest that RAG can exert a therapeutic effect on DMED by reducing hypoxic stress in the corpus cavernosum and increasing eNOS and iNOS levels. While our study yields promising results, it is not without its limitations. The complexity of traditional Chinese medicine ingredients makes it challenging to pinpoint which specific components contribute most to the therapeutic effects. Although our network pharmacology analysis identified some core active ingredients, further research is required to validate their roles. This study did not investigate the MAPK and cAMP signaling pathways, which are enriched in many targets and could play a role in the therapeutic effects of RAG. Further research is needed to explore the interaction of these pathways in the treatment process. Additionally, our research has only observed short-term effects and has not yet assessed the long-term efficacy and safety of RAG. Consequently, we plan to design more comprehensive experiments to validate our hypotheses.

Conclusions

In this study, we integrated network pharmacology, molecular docking, and an in vivo animal model to investigate the complex "component-target-disease" network relationship using a comprehensive system and holistic perspective. We also deeply explored the possibility of using RAG in the treatment of DMED. Our approaches provide a new direction for studying the mechanisms underlying the therapeutic effects of traditional Chinese medicine. Through bioinformatics analysis, we found INS, CAT, BDNF, CAPS3, CRP, and HMOX1 to be the core targets and the hypoxia-induced signaling pathway to be the key pathway. In addition, in vivo experiments demonstrated that RAG therapy alleviated DMED by improving the histopathological damage to the penile cavernous body and regulating the expression of related proteins (HIF-1, eNOS, iNOS, and HMOX1) in the cellular hypoxia-inducing pathway. Finally, this study showed that RAG reversed DMED, providing an alternative treatment method. However, further in vivo and in vitro studies are required to clarify the role and complex mechanisms of RAG in the treatment of DMED.

Data Sharing Statement

The published article and its supporting documents contain all the data generated or analyzed during this study.

Author Contributions

JXM and JFY conceived and participated in the study; JXM, JW and JH designed in vivo experiments and bioinformatics analysis ideas; YXG, JH, and JW conducted in vivo experiments; JW, and YXG analyzed network pharmacology and experiments data and wrote the manuscript. All authors reviewed the results and approved the final version of the manuscript.

Funding

This work was financially supported by the Zhejiang Provincial Natural Science Foundation of China (No. MS25H270044), the Zhejiang Province Traditional Chinese Medicine Inheritance and Innovation Talent Support Program(Nos.2025ZR071), the National Natural Science Foundation of China (Nos. 81804092, 82104855), Young

Elite Scientists Sponsorship Program by CACM (No. CACM-2022-QNRC2-A01), the 74th batch of general funding from the China Postdoctoral Science Foundation (No. 2023M743146) and Scientific Research Project Talent Program of Zhejiang Chinese Medical University (No. 2023RCZXZK47).

Disclosure

The authors report no conflicts of interest in this work.

References

1. Vita R, Benvenga S, Giammusso B, La Vignera S. Determinants of early response to low-intensity extracorporeal shockwaves for the treatment of vasculogenic erectile dysfunction: an open-label, prospective study. *J Clin Med*. 2019;8(7):1017–1028. doi:10.3390/jcm8071017
2. Defeudis G, Mazzilli R, Tenuta M, et al. Erectile dysfunction and diabetes: a melting pot of circumstances and treatments. *Diab Metab Res Rev*. 2022;38(2):e3494. doi:10.1002/dmrr.3494
3. Kouidrat Y, Pizzol D, Cosco T, et al. High prevalence of erectile dysfunction in diabetes: a systematic review and meta-analysis of 145 studies. *Diabet Med*. 2017;34(9):1185–1192. doi:10.1111/dme.13403
4. Malavige LS, Levy JC. Erectile dysfunction in diabetes mellitus. *J Sex Med*. 2009;6(5):1232–1247. doi:10.1111/j.1743-6109.2008.01168.x
5. Shamloul R, Ghanem H. Erectile dysfunction. *Lancet*. 2013;381(9861):153–165. doi:10.1016/S0140-6736(12)60520-0
6. Ouyang B, Xie Y, Zhang C, et al. Extracellular vesicles from human urine-derived stem cells ameliorate erectile dysfunction in a diabetic rat model by delivering proangiogenic microRNA. *Sex Med*. 2019;7(2):241–250. doi:10.1016/j.esxm.2019.02.001
7. Maxwell AJ. Mechanisms of dysfunction of the nitric oxide pathway in vascular diseases. *Nitric Oxide*. 2002;6(2):101–124. doi:10.1006/niox.2001.0394
8. Ryu JK, Suh JK, Burnett AL. Research in pharmacotherapy for erectile dysfunction. *Transl Androl Urol*. 2017;6(2):207–215. doi:10.21037/tau.2016.11.17
9. Bondeva T, Heinzig J, Ruhe C, Wolf G. Advanced glycated end-products affect HIF-transcriptional activity in renal cells. *Mol Endocrinol*. 2013;27(11):1918–1933. doi:10.1210/me.2013-1036
10. Glancy B, Hartnell LM, Combs CA, et al. Power grid protection of the muscle mitochondrial reticulum. *Cell Rep*. 2018;23(9):2832. doi:10.1016/j.celrep.2018.05.055
11. Ma H, Li Y, Hou T, et al. Sevoflurane postconditioning attenuates hypoxia/reoxygenation injury of cardiomyocytes under high glucose by regulating HIF-1α/MIF/AMPK pathway. *Front Pharmacol*. 2020;11:624809. doi:10.3389/fphar.2020.624809
12. Padmanabhan P, Mccullough AR. Penile oxygen saturation in the flaccid and erect penis in men with and without erectile dysfunction. *J Androl*. 2007;28(2):223–228. doi:10.2164/jandrol.106.001313
13. Lv B, Zhao J, Yang F, et al. Phenotypic transition of corpus cavernosum smooth muscle cells subjected to hypoxia. *Cell Tissue Res*. 2014;357(3):823–833. doi:10.1007/s00441-014-1902-0
14. Dwivedi PSR, Patil R, Khanal P, et al. Exploring the therapeutic mechanisms of Cassia glauca in diabetes mellitus through network pharmacology, molecular docking and molecular dynamics. *RSC Adv*. 2021;11(62):39362–39375. doi:10.1039/D1RA07661B
15. Tan YQ, Chen HW, Li J, Wu QJ. Efficacy, Chemical constituents, and pharmacological actions of Radix Paeoniae Rubra and Radix Paeoniae Alba. *Front Pharmacol*. 2020;11:1054. doi:10.3389/fphar.2020.01054
16. Le N, Zhou X, Fei WT, et al. Effects of Radix Paeoniae rubra, Radix Paeoniae Alba, paeoniflorin and albiflorin on hemorheology and vascular endothelial function in rats with acute blood stasis syndrome. *Global Tradit Chin Med*. 2019;12:1302–1307 doi:10.3969/j.issn.1674-1749.2019.09.002.
17. Huang CY, Kuo WW, Kuo CH, Tsai FJ, Liu PY, Hsieh DJY. Protective effect of Danggui (Radix Angelicae sinensis) on angiotensin II-induced apoptosis in H9c2 cardiomyoblast cells. *BMC Complement Altern Med*. 2014;14:358. doi:10.1186/1472-6882-14-358
18. Gong W, Zhu S, Chen C, et al. The anti-depression effect of angelicae sinensis radix is related to the pharmacological activity of modulating the hematological anomalies. *Front Pharmacol*. 2019;10:192. doi:10.3389/fphar.2019.00192
19. Luo Y, Wang Q, Zhang Y. A systems pharmacology approach to decipher the mechanism of danggui-shaoyao-san decoction for the treatment of neurodegenerative diseases. *J Ethnopharmacol*. 2016;178:66–81. doi:10.1016/j.jep.2015.12.011
20. Guo S, Wang G, Yang Z. Ligustilide alleviates the insulin resistance, lipid accumulation, and pathological injury with elevated phosphorylated AMPK level in rats with diabetes mellitus. *J Recept Signal Transduction Res*. 2021;41(1):85–92. doi:10.1080/10799893.2020.1789877
21. Hopkins AL. Network pharmacology: the next paradigm in drug discovery. *Nat Chem Biol*. 2008;4(11):682–690. doi:10.1038/nchembio.118
22. Shah U, Shah R, Acharya S, Acharya N. Novel anticancer agents from plant sources. *Chin J Nat Med*. 2013;11(1):16–23. doi:10.3724/SP.J.1009.2013.00016
23. Ru J, Li P, Wang J, et al. TCMSP: a database of systems pharmacology for drug discovery from herbal medicines. *J Cheminform*. 2014;6:13. doi:10.1186/1758-2946-6-13
24. Ma JX, Wang B, Li HS, et al. Uncovering the mechanisms of leech and centipede granules in the treatment of diabetes mellitus-induced erectile dysfunction utilising network pharmacology. *J Ethnopharmacol*. 2021;265:113358. doi:10.1016/j.jep.2020.113358
25. Tzeng TF, Liou SS, Liu IM. The selected traditional Chinese medicinal formulas for treating diabetic nephropathy: perspective of modern science. *J Tradit Complement Med*. 2013;3(3):152–158. doi:10.4103/2225-4110.114893
26. Xiaobing L, Chunling N, Wenyu C, Yan C, Zhenzhen L. Effect of Danggui-Shaoyao-San-containing serum on the renal tubular epithelial-mesenchymal transition of diabetic nephropathy. *Curr Pharm Biotechnol*. 2020;21(12):1204–1212. doi:10.2174/1389201021666200416094318
27. Loizou S, Lekakis I, Chrousos GP, Moutsatsou P. Beta-sitosterol exhibits anti-inflammatory activity in human aortic endothelial cells. *Mol Nutr Food Res*. 2010;54(4):551–558. doi:10.1002/mnfr.200900012
28. Bass VL, Soukup JM, Ghio AJ, Madden MC. Oleic acid and derivatives affect human endothelial cell mitochondrial function and vasoactive mediator production. *Lipids Health Dis*. 2020;19(1):128. doi:10.1186/s12944-020-01296-6

29. Martelli A, Flori L, Gorica E, et al. Vascular effects of the polyphenolic nutraceutical supplement Taurisolo®: focus on the protection of the endothelial function. *Nutrients*. 2021;13(5):1540. doi:10.3390/nu13051540
30. Babu S, Krishnan M, Rajagopal P, et al. Beta-sitosterol attenuates insulin resistance in adipose tissue via IRS-1/Akt mediated insulin signaling in high fat diet and sucrose induced type-2 diabetic rats. *Eur J Pharmacol*. 2020;873:173004. doi:10.1016/j.ejphar.2020.173004
31. Zhang Y, Liang Y, Liu H, Huang Y, Li H, Chen B. Paeoniflorin attenuates gestational diabetes via Akt/mTOR pathway in a rat model. *Food Nutr Res*. 2020;64:1 doi:10.29219/fnr.v64.4362.
32. Cengiz T, Kaya E, Oral DY, et al. Intracavernous injection of human umbilical cord blood mononuclear cells improves erectile dysfunction in streptozotocin-induced diabetic rats. *J Sex Med*. 2017;14(1):50–58. doi:10.1016/j.jsxm.2016.11.314
33. Cerychova R, Pavlinkova G. HIF-1, metabolism, and diabetes in the embryonic and adult heart. *Front Endocrinol*. 2018;9:460. doi:10.3389/fendo.2018.00460
34. Sagar SKD, Zhang C, Guo Q, Yi R, Yi R. Role of expression of endothelin-1 and angiotensin-II and hypoxia-inducible factor-1α in the kidney tissues of patients with diabetic nephropathy. *Saudi J Kidney Dis Transpl*. 2013;24(5):959–964. doi:10.4103/1319-2442.118098
35. Ayer A, Zarjou A, Agarwal A, Stocker R. Heme oxygenases in cardiovascular health and disease. *Physiol Rev*. 2016;96(4):1449–1508. doi:10.1152/physrev.00003.2016
36. He R, Wang Z, Cui M, et al. HIF1A alleviates compression-induced apoptosis of nucleus pulposus derived stem cells via upregulating autophagy. *Autophagy*. 2021;17(11):3338–3360. doi:10.1080/15548627.2021.1872227
37. Dunn LL, Kong SMY, Tumanov S, et al. Hmox1 (heme oxygenase-1) protects against ischemia-mediated injury via stabilization of HIF-1α (hypoxia-inducible factor-1α). *Arterioscler Thromb Vasc Biol*. 2021;41(1):317–330. doi:10.1161/ATVBAHA.120.315393
38. Ockaili R, Natarajan R, Salloum F, et al. HIF-1 activation attenuates postischemic myocardial injury: role for heme oxygenase-1 in modulating microvascular chemokine generation. *Am J Physiol Heart Circ Physiol*. 2005;289(2):H542–H548. doi:10.1152/ajpheart.00089.2005
39. Wang Z, Mao Y, Zang Y, et al. Transcriptomic analysis reveals the mechanism of isorhamnetin in the treatment of diabetes mellitus erectile dysfunction. *Free Radic Biol Med*. 2024;224:366–381. doi:10.1016/j.freeradbiomed.2024.08.043